COMPARATIVE ANALYSIS OF ELECTRON-PHONON COUPLING IN $LiCaAlF_6:Cr^{3+}$ AND $LiSrGaF_6:Cr^{3+}$★

N. M. AVRAM[1], M. G. BRIK[2], C. N. AVRAM[1], G. E. DRAGANESCU[1]

[1] Department of Physics, West University of Timisoara, Bd. V. Parvan 4, Timisoara 300223, Romania. E-mail: *avram@physics.uvt.ro*

[2] Fukui Institute for Fundamental Chemistry, Kyoto University, 34–4, Takano Nishihiraki-cho, Sakyo-ku, Kyoto 606–8103, Japan. E-mail: *brik@fukui.kyoto-u.ac.jp*

Received December 21, 2004

Electron-phonon coupling between optical electrons of the Cr^{3+} ion and crystal lattice vibration in $LiCaAlF_6$ and $LiSrGaF_6$ is studied using the single configurational coordinate model. The Huang-Rhys parameters and effective phonon energies were defined for both hosts using experimental spectroscopic data available in the literature. The dynamic Jahn-Teller effect is considered in details for $LiCaAlF_6:Cr^{3+}$; the Jahn-Teller stabilization energy was evaluated to be about 579 cm^{-1}, using two approaches: the Ham effect and geometry of the excited $^4T_{2g}$ electronic state.

Key words: crystal field theory; transition metal ions; electron-phonon interaction; the Jahn-Teller stabilization energy, Ham effect.

1. INTRODUCTION

Crystals activated by the Cr^{3+} ion are widely used as active media for solid state lasers. In fact, the very first laser was realized with $Al_2O_3:Cr^{3+}$ (ruby) [1]. Later on, a lot of other crystals were shown to lase with the Cr^{3+} ion; the number of them now is about 20, and the lasers based on these hosts cover the spectral region between 700 nm and 1100 nm [2, 3]. Such a wide tunability region is entirely due to the vibronic interaction between optical electrons of the Cr^{3+} ion and vibrations of the host lattice ions.

Crystals of $LiCaAlF_6$ and $LiSrGaF_6$ doped with Cr^{3+} were suggested as the laser hosts by Payne *et al.* [4, 5]. They are characterized by a high slope efficiency and almost temperature independent emission life time. The Cr^{3+} ion substitutes for the Al^{3+} and Ga^{3+} ions, respectively, and occupies the octahedral position, being surrounded by six F^- ions.

This work is a continuation of our previous studies of the title hosts [6–8]; here we report on the results of the comparative study of electron-phonon

★ Paper presented at the 5th International Balkan Workshop on Applied Physics, 5–7 July 2004, Constanța, Romania.

Rom. Journ. Phys., Vol. 50, Nos. 7–8, P. 795–806, Bucharest, 2005

interaction in both crystals, calculations of energy levels scheme and analysis of the Ham effect and the $^4T_{2g}$ excited state geometry changes produced by the dynamic Jahn-Teller effect.

2. PARAMETERS OF THE ELECTRON-PHONON INTERACTION

To study electron-phonon coupling of the Cr^{3+} ions with the lattice vibrations in both considered crystals, we used the single configurational coordinate model in harmonic approximation [9]. This model is based on the assumption that the nearest environment of the impurity ion oscillates harmonically about its equilibrium position. This displacement is described by the Q coordinate. Typical diagram of the potential energies of electronic states as a function of the

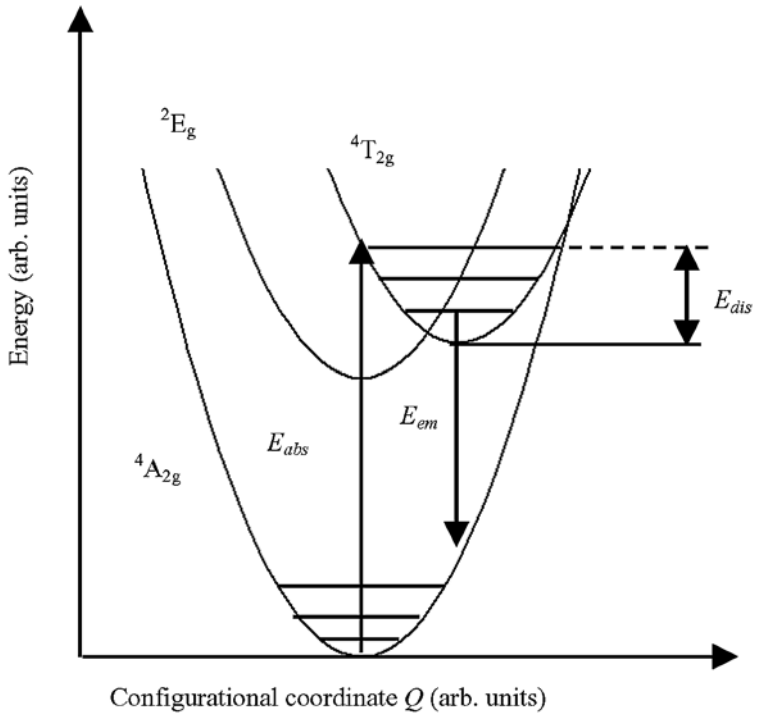

Fig. 1. – Single configurational coordinate diagram for $LiCaAlF_6:Cr^{3+}$ and $LiSrAlF_6:Cr^{3+}$ (schematic representation). The lowest electronic states are shown; the vibrational frequencies in all electronic states are assumed to be the same. Vibrational energy levels are indicated by horizontal lines. Absorption and emission transitions are indicated by the up-ward and down-ward arrows, respectively. The difference between the excited state vibrational level reached in the absorption transition and the minimum of the same parabola is denoted by E_{dis}.

vibrational coordinate Q for the case of a strong crystal field (when the orbital doublet ^2E is located below the orbital triplet $^4T_{2g}$) is sketched in Fig. 1.

Two main parameters which describe the electron-phonon coupling are the Huang-Rhys parameter S and the effective phonon energy $\hbar\omega$. The former is defined as the number of phonons of the energy $\hbar\omega$ excited in the absorption transition [9]:

$$S = \frac{E_{dis}}{\hbar\omega} \tag{1}$$

(where E_{dis} is defined in Fig. 1). Both parameters S and $\hbar\omega$ are related to the difference between the first absorption and corresponding emission bands peaks (energetical Stokes shift) ΔE by the following expression [9–10]:

$$\Delta E = (2S - 1)\hbar\omega\,. \tag{2}$$

The second equation which is required for to calculate the values of S and $\hbar\omega$ is as follows [9, 10]:

$$\Gamma(T) = 2.35\hbar\omega\sqrt{S\coth\left(\frac{\hbar\omega}{2kT}\right)}, \tag{3}$$

where $\Gamma(T)$ is the full width at half maximum (FWHM) at the absolute temperature T. In order to solve the system of equations (2)–(3) we used the spectroscopic data from [4–5]. According to these data for $LiSrGaF_6:Cr^{3+}$, the energetical Stokes shift ΔE between maxima of the $^4A_{2g} - {}^4T_{2g}$ absorption and corresponding $^4T_{2g} - {}^4A_{2g}$ emission is about 3649 cm^{-1}, and the FWHM of the $^4T_{2g} - {}^4A_{2g}$ emission band at 295 K is about 2760 cm^{-1}. Solving equations (2)–(3) yields in the following values: $S = 3.65$, $\hbar\omega = 580$ cm^{-1}.

According to similar data for $LiCaAlF_6:Cr^{3+}$, the energetical Stokes shift ΔE is about 2653 cm^{-1}, and the FWHM of the $^4T_{2g} - {}^4A_{2g}$ emission band at 295 K is about 2070 cm^{-1}. These data produce the following values of the parameters of electron-phonon coupling: $S = 4.19$, $\hbar\omega = 359$ cm^{-1}.

The obtained results for the Stokes shifts will be used for the analysis of the Jahn-Teller effect.

3. THE HAM EFFECT IN THE $^4T_{2G}$ STATE: THE $T \otimes e$ INTERACTION IN $LiCaAlF_6:Cr^{3+}$

Due to an interaction between optical electrons of an impurity ion and Jahn-Teller active vibrational modes, the observed spin-orbit (SO) splitting of the orbital triplet states is reduced several times in magnitude, compared to the splitting which is expected to be from the theoretical calculations. This is known

as the Ham effect [11], and serves as a firm experimental evidence of the Jahn-Teller effect. Comparison of the experimental and calculated SO splittings of the orbital triplets gives a possibility of the direct evaluation of the Jahn-Teller stabilization energy E_{JT} for the considered complex. It is convenient to express the calculated SO splittings in terms of the dimensionless parameter

$$\gamma = \exp\left(-\frac{3E_{JT}}{2\hbar\omega}\right), \tag{4}$$

where $\hbar\omega$ stands for the energy of the Jahn-Teller active mode (which here and thereafter is assumed to be the e_g normal mode) it interacts more strongly with the electronic states than other normal modes of the octahedral complex. For $LiCaAlF_6$ $\hbar\omega_{e_g} = 452$ cm^{-1} [12]). Below, in Table 1, the results of the calculations of the SO splitting of the $^4T_{2g}$ state of the Cr^{3+} ion in $LiCaAlF_6$ are given, along with experimental data [7].

Table 1

Relative energy (in cm^{-1}) of the four SO components of the $^4T_{2g}$ state in $LiCaAlF_6$:Cr^{3+}

O_h double group irreducible representation	a	B	c
Γ_7	0	0	0
Γ_8	130	19	14
Γ_6	309	45	48
Γ'_8	410	60	60

(a) Calculation using the full d^3 matrix [13, 14] with the following parameters (all in cm^{-1}): $Dq = 1476$, $B = 686$, $C = 3090$, $\xi_{SO} = 218$.
(b) Calculation including the Jahn-Teller effect with the Ham parameter $\gamma = 1.92$.
(c) Experimentally observed relative energies [12].

As it can be seen from Table 1, taking into account the Ham reduction effect improves significantly the correspondence between calculated and observed splittings. The Jahn-Teller stabilization energy E_{JT} can readily be estimated from Eq. (4) to be 579 cm^{-1} (what is in a favorable agreement with an experimental result $E_{JT} = 600$ cm^{-1} [15]). The non-dimensional Stokes shift for the e_g normal mode is $S_{e_g} = E_{JT}/\hbar\omega_{e_g} = 1.28$.

4. GEOMETRY OF THE $^4T_{2G}$ EXCITED STATE IN $LiCaAlF_6$:Cr^{3+}

As a result of different bonding properties in the ground and excited states of an impurity ion in a crystal, they may have different geometries, what is

revealed in the shift of the potential energy surfaces of the considered electron states. In order to perform a qualitative analysis of this phenomenon, we use the effective Hamiltonian H_{VIB} which describes the interaction of the electron states with the lattice normal modes in the form

$$H_{VIB} = \sum_i \left[\frac{P_i^2}{2\mu_i} + \frac{1}{2} K_i Q_i^2 + \left(\frac{\partial V}{\partial Q_i} \right)_0 Q_i \right]. \tag{5}$$

Here μ_i is the effective mass of the *i*-th vibration and P_i is the momentum conjugate to the corresponding normal vibrational coordinate Q_i. The first two terms transform the electronic levels into potential energy manifolds in the coordinates of the octahedral normal modes Q_i with vibrational frequencies $\omega_i = \sqrt{K_i/\mu_i}$, and the complete wave functions in the Born-Oppenheimer approximation can be written as a product of an electronic and a vibrational parts. The third term can be understood as a force F_i, which acts along the vibrational mode Q_i associated with the electronic state Γ:

$$F_i = -\left\langle \Gamma \left| \frac{\partial V}{\partial Q_i} \right|_0 \Gamma \right\rangle, \tag{6}$$

where the subscript means that the derivative is to be found at the equilibrium configuration. This force is balanced by the harmonic restoring force $K_i \Delta Q_i$ at the distorted geometry

$$\Delta Q_i = -\frac{F_i}{K_i}. \tag{7}$$

This distortion lowers the energy of the electronic state by an amount

$$E_i = \frac{1}{2} K_i \left(\Delta Q_i \right)^2 \tag{8}$$

comparing to the equilibrium position. Group theory predicts that only distortions along the a_{1g}, e_g, t_{2g} octahedral modes are important for the $^4T_{2g}$ electron state. The Hamiltonian (5) can be rewritten in basis consisting of the ξ, η, ζ real orbitals:

$$H_{VIB} = \sum_i \left(\frac{P_i^2}{2\mu_i} + \frac{1}{2} K_i Q_i^2 \right) + \left\langle {}^4T_{2g} \left\| \frac{\partial V}{\partial Q_{a_{1g}}} \right\| {}^4T_{2g} \right\rangle \begin{pmatrix} Q_{a_{1g}} & 0 & 0 \\ 0 & Q_{a_{1g}} & 0 \\ 0 & 0 & Q_{a_{1g}} \end{pmatrix} +$$

$$+\left\langle {}^4T_{2g}\left\|\frac{\partial V}{\partial Q_{e_g}}\right\|{}^4T_{2g}\right\rangle\begin{pmatrix}\frac{1}{2}Q_{e_{g\theta}} & -\frac{\sqrt{3}}{2}Q_{e_{g\varepsilon}} & 0 & 0\\ 0 & \frac{1}{2}Q_{e_{g\theta}}+\frac{\sqrt{3}}{2}Q_{e_{g\varepsilon}} & 0\\ 0 & 0 & -Q_{e_{g\theta}}\end{pmatrix}+$$
$$+\left\langle {}^4T_{2g}\left\|\frac{\partial V}{\partial Q_{t_{2g}}}\right\|{}^4T_{2g}\right\rangle\begin{pmatrix}0 & Q_{t_{2g\zeta}} & Q_{t_{2g\eta}}\\ Q_{t_{2g\zeta}} & 0 & Q_{t_{2g\xi}}\\ Q_{t_{2g\eta}} & Q_{t_{2g\xi}} & 0\end{pmatrix}. \tag{9}$$

In this equation the reduced matrix elements in the front of the parenthesis represent the vibronic coupling constants between the triple degenerate electronic state ${}^4T_{2g}$ and the normal vibration modes a_{1g}, e_g, t_{2g}, respectively. The indices θ, ε and ξ, η, ζ are used to distinguish between different normal modes of the e_g and t_{2g}, respectively. They can be evaluated using explicit expressions obtained in [16]:

$$\left\langle {}^4T_{2g}\left\|\frac{\partial V}{\partial Q_{a_{1g}}}\right\|{}^4T_{2g}\right\rangle=-\frac{50}{\sqrt{6}R_o}Dq, \tag{10}$$

$$\left\langle {}^4T_{2g}\left\|\frac{\partial V}{\partial Q_{e_g}}\right\|{}^4T_{2g}\right\rangle=-\frac{25}{R_0\sqrt{3}}Dq, \tag{11}$$

$$\left\langle {}^4T_{2g}\left\|\frac{\partial V}{\partial Q_{t_{2g}}}\right\|{}^4T_{2g}\right\rangle=-\frac{18\sqrt{2}}{7R_0}Dq\left(\frac{1}{\eta}-\frac{5}{9}\right), \tag{12}$$

where Dq is the crystal field strength, $R_0 = 1.8$ Å is the equilibrium distance between the Cr^{3+} and F^- ions [17], and [16]

$$\eta=\left(\frac{\langle r^2\rangle {R_0}^2}{\langle r^4\rangle}\right)^{-1}=\frac{3}{5}\frac{3-4\,e_\pi/e_\sigma}{1+e_\pi/e_\sigma}, \tag{13}$$

with the angular overlap model parameters e_π and e_σ defined in [18]. Using the value of Dq from the third section, and the ratio $e_\pi/e_\sigma = 0.31$ for the $[CrF_6]^{3-}$ cluster [18], we got for these constants the following numerical values:

$$\left\langle {}^4T_{2g}\left\|\frac{\partial V}{\partial Q_{a_{1g}}}\right\|{}^4T_{2g}\right\rangle=-0.33\times10^{-8}\,N,\ \left\langle {}^4T_{2g}\left\|\frac{\partial V}{\partial Q_{e_g}}\right\|{}^4T_{2g}\right\rangle=-0.26\times10^{-8}\,N,$$

$$\left\langle {}^4T_{2g} \left\| \frac{\partial V}{\partial Q_{t_{2g}}} \right\| {}^4T_{2g} \right\rangle = -0.41\times 10^{-9}\ N.$$

As can be seen from the structure of Eq. (9), the coupling with the fully symmetric a_{1g} mode is diagonal, producing an overall shift of all three electron states in the $Q_{a_{1g}}$ space. The coupling with the e_g normal mode is also diagonal, but it results in the splitting of the three electron state and displacements of all its components along different directions in the $Q_{e_g\theta}$, $Q_{e_g\varepsilon}$ space. The direct comparison of the electron-phonon coupling constants shows that the coupling with the t_{2g} normal mode is the weakest among all the modes, and can be safely neglected.

The equilibrium magnitude $\left|\Delta Q_i\right|_{eq}$ of the i-th normal mode with energy $\hbar\omega_i$ is related to the Stokes shift S_i and force constant K_i by the following equation [19]:

$$\left|\Delta Q_i\right|_{eq} = \left[\frac{2S_i\hbar\omega_i}{K_i}\right]^{1/2}. \tag{14}$$

The force constants K_i were calculated with the FG matrix method for an octahedral MX_6 molecule [20]. With $\hbar\omega_{a_{1g}} = 561$ cm^{-1} and $\hbar\omega_{e_g} = 452$ cm^{-1} [12] we got that the corresponding force constants are $K_{a_{1g}} = 258.0$ N/m and $K_{e_g} = 167.5$ N/m. The Huang-Rhys factor $S_{e_g} = 1.28$ has been estimated in the second section. Neglecting the vibronic coupling to the t_{2g} normal mode, the Huang-Rhys factor $S_{a_{1g}}$ for the fully symmetric mode can be estimated as $S_{a_{1g}} = S - S_{e_g} = 4.19 - 1.28 = 2.91$ (here the results of the third section were used). Using this data, we got $\left|\Delta Q_{a_{1g}}\right|_{eq} = 0.159$ Å and $\left|\Delta Q_{e_g}\right|_{eq} = 0.117$ Å. As previously demonstrated, based on the group theoretical considerations, the sign of the $\left|\Delta Q_{a_{1g}}\right|_{eq}$ should be positive, whereas the sign of the $\left|\Delta Q_{e_g}\right|_{eq}$ is negative [21]. It is more convenient to express the character of the ligands displacements in terms of the interatomic bonds changes. It is well known that in the $T_{2g}\otimes e_g$ case the three potential wells of the ${}^4T_{2g}$ components ξ, η, ζ are spatially separated, *i.e.* each of these three components distorts along a different direction in the $Q_{e_g\theta}$, $Q_{e_g\varepsilon}$ space. All these components are related by symmetry and, therefore, it is sufficient to consider just one single component for the further

detailed analysis. The coordinate system in the $Q_{e_g\theta}$, $Q_{e_g\varepsilon}$ space can always be chosen such, that the the potential minimum of the considered $^4T_{2g}$ component (anyone from ξ, η, ζ) lies on the Q_θ axis (this means, no distortion takes place along the Q_ε axis). Then it is possible to consider the $\left|\Delta Q_{e_g}\right|_{eq}$ values as corresponding to $\left|\Delta Q_{e_g\theta}\right|_{eq}$, whereas $\left|\Delta Q_{e_g\varepsilon}\right|_{eq}$ is zero. Using the transformation matrix, which can be easily obtained from the explicit expressions for the normal vibrations of the octahedral complex [21] (the equilibrium subscript "eq" is suppressed in this equation)

$$\begin{pmatrix}\Delta x\\ \Delta y\\ \Delta z\end{pmatrix}=\frac{1}{2}\begin{pmatrix}\sqrt{\frac{2}{3}} & -\sqrt{\frac{1}{3}} & -1\\ \sqrt{\frac{2}{3}} & -\sqrt{\frac{1}{3}} & 1\\ \sqrt{\frac{2}{3}} & \sqrt{\frac{4}{3}} & 0\end{pmatrix}\begin{pmatrix}\Delta Q_{a_{1g}}\\ \Delta Q_{e_g\theta}\\ \Delta Q_{e_g\varepsilon}\end{pmatrix}, \tag{15}$$

the values of the $\left|\Delta Q_{a_{1g}}\right|_{eq}$ and $\left|\Delta Q_{e_g\theta}\right|_{eq}$ can be converted into the changes in the metal–ligand bond lengths Δx_{eq}, Δy_{eq}, Δz_{eq}, which are presented in Table 2, along with ΔQ_i. The combined effect of both a_{1g} and e_g normal modes is a net equatorial expansion and a slight axial compression of the fluorine octahedron, as is depicted in Fig. 2.

Table 2

Huang-Rhys factors and equilibrium geometries of the $[CrF_6]^{3-}$ octahedron in the $^4T_{2g}$ excited state relative to the $^4A_{2g}$ ground state in $LiCaAlF_6:Cr^{3+}$

$S_{a_{1g}}$	2.91	$\Delta Q_{a_{1g},eq}$, [Å]	0.159	Δx_{eq}, Δy_{eq} [Å]	0.099
S_{e_g}	1.28	$\Delta Q_{e_g,eq}$, [Å]	–0.117	Δz_{eq}, [Å]	–0.003

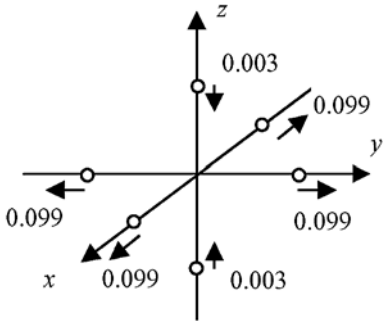

Fig. 2. – Distortion of the $[CrF_6]^{3-}$ complex in the $^4T_{2g}$ excited state with respect to the ground state (directions of the displacements and their magnitudes in Å are shown by arrows and numbers, respectively).

These distortions should not be understood as a static lowering of the point symmetry from O_h in the ground $^4A_{2g}$ state to D_{4h} in the excited $^4T_{2g}$ state along a given axis in the crystal. This is dynamical distortion, which takes place along each of the three axes of the octahedral cluster $[CrF_6]^{3-}$. Similar analysis which was performed for the Cr^{3+} ion in the $Cs_2NaScCl_6$ [22] resulted in analogous

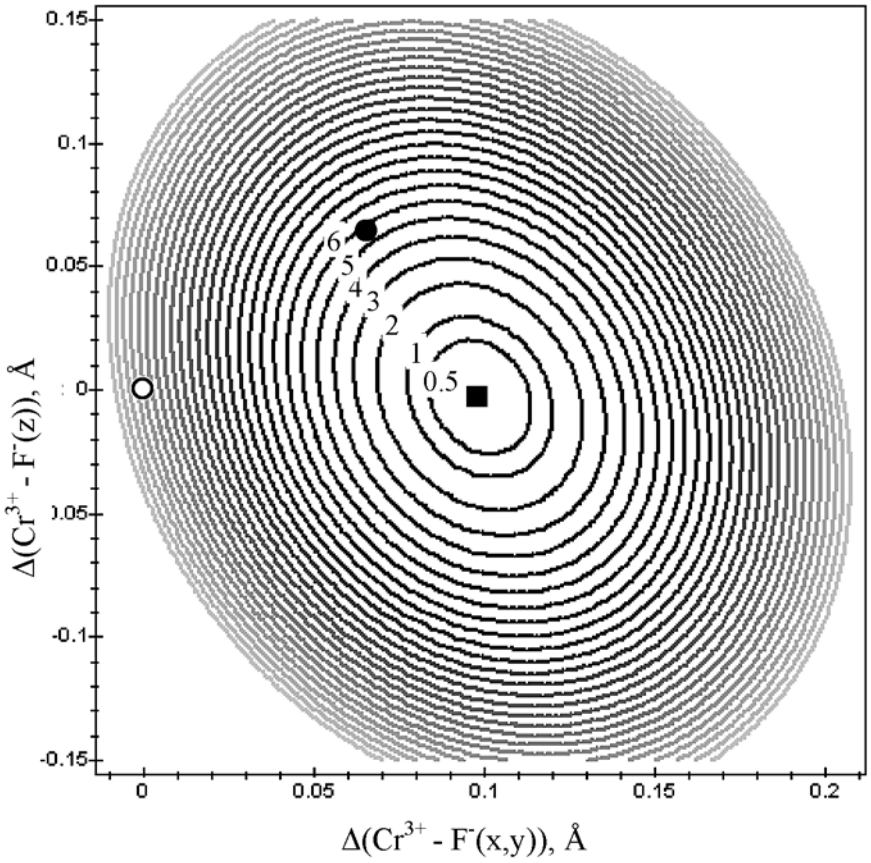

Fig. 3. – Contour plot of the harmonic $^4T_{2g}$ potential energy surface for the $LiCaAlF_6:Cr^{3+}$ system as a function of changes in Cr^{3+}–$F^-(x, y)$ and Cr^{3+}–$F^-(z)$ chemical bonds lengths. The energies of individual contours are given in hundreds of wave numbers. The open circle at the origin corresponds to the equilibrium position of the ground $^4A_{2g}$ potential energy surface; the black square indicates the equilibrium position of the $^4T_{2g}$ potential energy surface shifted with respect to the ground state as a combined result of the a_{1g} and e_g normal vibrations. The black circle shows the hypothetical position of $^4T_{2g}$ potential energy surface minimum if there were no e_g normal vibration (*i.e.* in the absence of the Jahn-Teller distortion). The value on the potential energy surface of the $^4T_{2g}$ state at this point (between 500 and 600 cm^{-1} from the figure) corresponds to the Jahn-Teller energy for the considered complex. Details of calculations are given in the text.

character of the dynamical deformations of the octahedral cluster formed around the Cr^{3+} ion.

After the force constants and amplitudes of the ionic displacements are found, it is possible to draw the potential energy surface of the ${}^4T_{2g}$ excited electronic state. In the harmonic approximation, this energy is described by the following expression:

$$V = \frac{1}{2} K_{a_{1g}} \left(\Delta Q_{a_{1g}} - \Delta Q_{a_{1g},eq} \right)^2 + \frac{1}{2} K_{e_g} \left(\Delta Q_{e_g} - \Delta Q_{e_g,eq} \right)^2. \tag{16}$$

An inverse to the Eq. (15) transformation should be used to get the dependence of the potential energy on the changes of the interionic distances. The contour plot of the potential energy surface in the ${}^4T_{2g}$ state is shown in Fig. 3.

In Fig. 3 the equilibrium position of the ground state is indicated by the open circle, the equilibrium position of the excited state is shown by the black square. Neglecting the interaction with the e_g normal mode (this means $S_{e_g} = 0$), we found the values of the Δx, Δy, Δz displacements produced by the full-symmetric vibration a_{1g} to be $\Delta x = \Delta y = \Delta z = 0.065$ Å. This position is shown in Fig. 3 by the black circle. Using these coordinates in Eq. (16), the Jahn-Teller stabilization energy can be readily estimated to be 578 cm^{-1}, in an excellent agreement with the result obtained from the SO splitting quenching caused by the Ham effect.

5. CONCLUSION

Detailed analysis of the electron-phonon coupling in two fluoride crystals doped with trivalent chromium: $LiCaAlF_6:Cr^{3+}$ and $LiSrGaF_6:Cr^{3+}$ crystal was performed in this paper. Using experimental spectroscopic data from [4, 5], the Stokes shifts and effective phonon energies were determined to be $S = 4.19$, $\hbar\omega = 359$ cm^{-1} for $LiCaAlF_6:Cr^{3+}$ and $S = 3.65$, $\hbar\omega = 580$ cm^{-1} for $LiSrGaF_6:Cr^{3+}$. The dynamic Jahn-Teller effect in the ${}^4T_{2g}$ excited state of the Cr^{3+} ion in $LiCaAlF_6$ was considered. The Jahn-Teller stabilization energy E_{JT} was evaluated to be about 579 cm^{-1}, the value, which is in a good agreement with experimental data ($E_{JT} = 600$ cm^{-1}, [15]). Detailed analysis of the structure of the linear vibronic Hamiltonian, including numerical estimations of the constants of the electron-phonon coupling, was performed. This analysis supplied with the estimation of the force constants for the Jahn-Teller active modes, gave a possibility to estimate the equilibrium displacements of the ligands due to the combined result of the a_{1g} and e_g normal modes. It was shown that the net result of both vibrations is an equatorial expansion by 0.099 Å and an axial compression by 0.003 Å. Finally, the contour plot of the potential

surface energy in the $^4T_{2g}$ electron state has been plotted; the Jahn-Teller stabilization energy estimated from the obtained plot turned out to be 578 cm^{-1}, what agrees excellently with the results obtained from application of the Ham theory.

Acknowledgments. M. G. Brik appreciates financial support from the Japanese Ministry of Education, Culture, Sports, Science and Technology (MEXT) in a project on computational materials science unit at Kyoto University.

REFERENCES

1. T. H. Maiman, *Optical and Microwave-Optical Experiments in Ruby*, Phys. Rev. Lett., 4, 564–566, (1960).
2. S. Kück, *Laser-related spectroscopy of ion-doped crystals for tunable solid-state lasers*, Appl. Phys. B, 72**,** 515–562, (2001).
3. A. A. Kaminskii, *Modern developments in the physics of crystalline laser materials*, Phys. Stat. Solidi (a), 200, 215–296, (2003).
4. S. A. Payne, L. L. Chase, H. W. Newkirk, L. S. Smith, and W. F. Krupke, *$LiCaAlF_6:Cr^{3+}$: a promising new solid-state laser material*, IEEE J. Quantum Electron., 24, 2243–2252, (1988).
5. L. K. Smith, S. A. Payne, W. L. Kway, L. L. Chase, and B. H. T. Chai, *Investigation of the Laser properties of Cr^{3+}:$LiSrGaF_6$,* IEEE J. Quantum Electron., 28, 2612–2618, (1988).
6. M. G. Brik, C. N. Avram, N. M. Avram, *Linear electron-phonon interaction and non-radiative transitions in $LiCaAlF_6:Cr^{3+}$ laser crystals*, OSA Trends in Optics and Photonics Vol. 68, Advanced Solid-State Lasers, Martin E. Fermann and Larry R. Marshall, eds. (Optical Society of America, Washington, DC 2002), pp. 275–279.
7. C. N. Avram, M. G. Brik, *Manifestation of vibronic interaction in the fine structure of Cr^{3+} energy levels in laser crystal $LiCaAlF_6:Cr^{3+}$*, J. Lumin., 102–103, 81–84, (2003).
8. M. G. Brik, C. N. Avram, *Comparative analysis of non-radiative relaxation of Cr^{3+} in $LiCaAlF_6$ and Al_2O_3 crystals*, J. Lumin., 102–103, 283–286, (2003).
9. B. Henderson and G. F. Imbush, *Optical Spectroscopy of Inorganic Solids*, Clarendon Press, Oxford, 1989.
10. G. A. Torchia, O. Martinez-Matos, N. M. Khaidukov, J. O. Tocho, *Phonon coupling of Cr^{3+} ions in Cs_2NaAlF_6 crystals*, Solid State Commun., 130, 159–163, (2004).
11. F. S. Ham, *Dynamical Jahn-Teller effect in paramagnetic resonance spectra: orbital reduction factors and partial quenching of spin-orbit interaction*, Phys. Rev., 138, A1727–A1740, (1965).
12. S. A. Payne, L. L. Chase, G. D. Wilke, *Optical spectroscopy of the new laser materials, $LiSrAlF_6:Cr^{3+}$ and $LiCaAlF_6:Cr^{3+}$*, J. Lumin., 44, 167–176, (1989).
13. J. C. Eisenstein, *Magnetic properties and optical absorption spectrum of K_2ReCl_6*, J. Chem. Phys., 34, 1628–1648, (1961).
14. M. Grinberg, *$^2E\,^4A_2$ fluorescence of Cr^{3+} in high and intermediate field garnets,* J. Lumin., 54, 369–382, (1993).
15. H. W. H. Lee, S. A. Payne, L. L. Chase, *Excited-state absorption of Cr^{3+} in $LiCaAlF_6$: Effects of asymmetric distortions and intensity selection rules*, Phys. Rev. B, 39, 8907–8914, (1989).
16. K. Wissing, J. Degen, *Calculation of vibronic coupling constants for tetrahedral and octahedral d electron systems via dynamic ligand field theory and application to optical spectra*, Mol. Physics, 95, 51–59, (1998).
17. V. W. Viebahn, *Untersuchungen an Quaternären Fluoriden $LiMeMeF_6$, Die Struktur vor $LiCaAlF_6$*, Z. Anorg. Allg. Chem., 386, 335–339, (1971).

18. T. Schönherr, *Angular overlap model applied to transition metal complexes and d^N-ions in oxide host lattices*, Topics current Chem., 191, 87–152, (1997).
19. T. C. Brunold, H. U. Güdel, in: *Inorganic Electronic Structure and Spectroscopy*, vol. I: Methodology, Eds. E. I. Solomon and A. B. P. Lever, John Wiley & Sons, Inc, 1999.
20. K. Venkateswarlu and S. Sundaram, *Evaluation of Force Constants: Molecules of the type XY_6*, Phys. Chem. Neue Folge, 9, 174–179, (1956).
21. R. B. Wilson and E. I. Solomon, *Spectroscopic studies of the photoactive $^4T_{2g}$ excited state of hexaamminechromium (III)*, Inorg. Chem., 17, 1729–1736, (1978).
22. O. S. Wenger and H. U. Güdel, *Optical spectroscopy of $CrCl_6^{3-}$ doped $Cs_2NaScCl_6$: broadband near-infrared luminescence and Jahn-Teller effect*, J. Chem. Phys., 114, 5832–5841, (2001).